

Optical characterisation of ilmenite by reflectance spectroscopy

Jingjing Chen^a, Xiaobo Yin^a

^a*Department of Mechanical Engineering, The University of Hong Kong, Hong Kong, China*

Abstract

Bi-directional reflectance spectroscopy based on multiple scattering of particulate surfaces is employed in identifying the optical properties of ilmenite from laboratory reflectance measurements. However, the approach suffers from issues including: i) both n and k are to be extracted from a single spectroscopy spectrum, ii) imposing constraints of the Kramers–Kronig correlation relating spectral n and k is weakened by its fundamental insensitivities, and iii) incapability in addressing intrinsic strong absorption features of absorbing materials. We resolve these issues by employing additional optical information of directional–hemispherical reflectance and emissivity/absorptivity for a slab and a stratified multi-layer medium of the material, respectively. The accompanied analyses consist of radiative transfer in a slab medium investigated using the two-flux approximation method and electromagnetic radiation propagation in a stratified multi-layer medium investigated using the electric field transfer matrix. We further find that an understanding of the internal scattering coefficient of grains in the multiple scattering model paves the way in successfully predicting absorption features of materials. A wavelength-dependent internal scattering coefficient of ilmenite is then found to be $50 \mu\text{m}^{-1}$ and $10^{-7} \mu\text{m}^{-1}$ in regions of strong absorption ($<7 \mu\text{m}$, $>13 \mu\text{m}$) and high transmission ($7\text{--}13 \mu\text{m}$), respectively. The value of the refractive index n varies weakly on the wavelength. A pronounced change in the determined absorptive index k with the wavelength is observed. Low values of the absorptive index k on the magnitude of 10^{-2} are obtained in the transmission window spectral range. In the strong absorption spectral range starting from $13 \mu\text{m}$, values of the absorptive index k are higher than 0.1.

Keywords: Radiative transfer, Multiple scattering, Reflectance spectroscopy, Two-flux approximation, N -phase multi-layer

*

Email addresses: jchen022@hku.hk (Jingjing Chen), xbyin@hku.hk (Xiaobo Yin)

1. Introduction

Detailed optical properties (refractive index n and absorptive index k) of materials are necessary for forward modelling of spectra which is to calculate the spectrum of a designed phase mixture as employed in developing photonic materials [3, 5, 18, 23, 24] and inverse modelling which is to extract the properties from the spectrum of a remotely observed surface as encountered in reflectance spectroscopy [1, 2, 7, 16]. The frequently used method for determining optical properties of materials is depositing a thin film on a substrate by sputtering techniques and then identifying the properties using ellipsometry by measuring the change in the polarization state as light reflects from the thin film surface [11]. However, materials such as ilmenite cannot be evaporated and deposited in a uniform coating, thus ruling out ellipsometry as a determination method [20]. An alternative approach, which is a combination of measurements of bi-directional reflectance of particulate media and subsequent analysis of radiative transfer within using the multiple scattering theory, was proposed by Hapke [10]. Considering both n and k are to be determined from a single reflectance spectrum, currently, the standard approach is employing a constant n , which is taken from existing reference data of the material, and iteratively varying k to make the calculated and measured reflectance spectrum to agree with each other. Roush [21] later improved this approach by subsequently using a subtractive Kramers–Kronig analysis to allow determination of n as a function of wavelength. However, this handling of n requires a prior understanding of investigated materials, and suffers from fundamental insensitivity to spectral features and changes in k across the entire spectral range. The approach has been applied to determine the optical properties of transparent [4, 12, 15, 19, 21] and opaque materials [20]. However, it is recognized that the approach provides a poor determination of the optical properties in infrared regions where absorbing materials exhibit strong absorption specifications [20, 21].

In this work, we aim to resolve these issues encountered in the standard reflectance spectroscopy approach based on the Hapke radiative transfer model and identify the optical properties of dark, opaque ilmenite. For solving the issue of two unknowns n , k to be determined from a single reflectance spectrum for powdered materials, additional information of radiative transfer in a slab medium is introduced. Specifically, the determination of the refractive index n is achieved by a distinct reflectance spectroscopy for the pellet material. By considering the pellet as a plane-parallel slab medium, the radiative transfer within is analyzed using the two-flux approximation method [6, 8, 14, 17], and the directional–hemispherical reflectance is found to be a function of the refractive index n of materials. For solving the issue of incapable of identifying strong absorption characteristics in the standard Hapke model, a thorough investigation on the radiative properties involved in the model is conducted. Specifically, the internal scattering coefficient parameter which is neglected in the standard approach turns out to be the key. In addition, the validation

of the investigation on the parameter and the combined reflectance spectroscopy is provided by scrutinizing the absorptivity/emissivity of the thin film media by embedding the particulate material into transparent plastic matrix. The proposed approach is then employed to identify the optical properties of opaque ilmenite.

2. Measurement Data

Three types of samples made from ilmenite—particulate, pellet, and film—are used for investigating the optical properties of ilmenite in this study. The bi-directional reflectance, directional-hemispherical reflectance, and absorptivity/emissivity are obtained for the particulate, pellet, and film media, respectively.

2.1. Bi-directional reflectance of particulate media

The RELAB online spectral library archives spectral data and sample preparation, characterization, acquisition, and spectral measurements. Assuming the composition is independent of grain size, additional leverage is achieved by using reflectance spectra of two different grain sizes of ilmenite. The ilmenite powder samples investigated in this study are 0–30 μm (IL-M1O-005) and 0–45 μm (IL-LPK-007). Bi-directional reflectance spectra are for incidence and emission angles of 30° and 0° , respectively. The bi-directional reflectance of particulate ilmenite with the two particle size distributions is shown in Fig. 1. More details on the measurement approach can be found in The RELAB spectral library and [21].

2.2. Directional-hemispherical reflectance of pellet media

Similarly, Bi-directional reflectance for pellet ilmenite (IL-LPK-007-P) is obtained from RELAB spectral library (see Fig. 2). The directional-hemispherical reflectance is calculated using Shkuratov and Grynko relation $\log R_{\text{d-d}} = 1.088 \log R_{\text{d-h}}$ [22], where $R_{\text{d-d}}$ and $R_{\text{d-h}}$ are bi-directional and directional-hemispherical reflectance, respectively. The effect of material volume fraction on the relation is neglected and detailed analysis is beyond the scope of the current paper. The resulting data is also plotted in Fig. 2.

2.3. Emissivity/absorptivity of film media

The ilmenite and low-density polyethylene powders are mixed at a volume ratio of 1:9. The film material with a thickness of 50 μm on aluminium is fabricated by hot-pressing the mixed powder at 160°C and 25 MPa onto a highly reflecting aluminium for 10 seconds. The spectral reflectance of the film fabricated in the solar spectrum (0.3–2.5 μm) and mid-infrared (2.5–25 μm)

are characterized using UV-VIS-NIR spectrophotometer (Cary 5000, Agilent) equipped with an integrating sphere (DRA-2500, Agilent) and Fourier transform infrared spectrometer (Nicolet is50) with a gold-coated integrating sphere (PIKE technologies), respectively. Employing the Kirchoff's law, the emissivity/absorptivity is obtained as $\epsilon = A = 1 - R$ and shown in Fig. 3, where ϵ , A , and R are emissivity, absorptivity, and reflectance, respectively.

3. Analytic methods

The phenomena involved in determining and evaluating optical constants of materials in this work consist of light propagation and interaction in particulate, slab, and multi-layer media. For the particulate media, an analysis of the radiative transfer within describing the scattering of light from particulate surfaces is performed [10]. The resulting analytic solution relates bi-directional reflectance with the single scattering albedo and the single scattering albedo with the optical constants. For investigating radiative transfer in the plane-parallel slab of medium, the two-flux approximation is employed and the result of directional-hemispherical reflectance is obtained as a function of the refractive index of the material [6, 8]. The emissivity/absorptivity data of the multi-layer film is scrutinized for revealing and evaluating the absorption features of the material in the infrared region. Its underlying physics involved is light propagation in a multi-layer medium and electric fields induced by plane electromagnetic radiation within are derived [9].

3.1. Analysis of radiative transfer in particulate media by the multiple scattering theory

For a plane surface containing absorbing particles, the medium is illuminated by collimated light traveling into direction with an incidence angle of $\pi - \theta_i$. The medium is observed with an emission angle of θ_e . The description of light attenuation and scattering from individual particulate surface is schematically shown in Fig. 4. Assuming that the particles are irregular and arranged with no particular orientation, coherent effects average out. Taking multiple scattering, mutual shadowing and opposition effects into account, the bi-directional reflectance is obtained as [10],

$$R_{d-d} = \frac{\omega}{4\pi} \frac{\mu_0}{\mu_0 + \mu} \{ [1 + B(g)] \Phi(g) + H(\mu_0)H(\mu) - 1 \}, \quad (1)$$

where $\mu_0 = \cos \theta_i$, $\mu = \cos \theta_e$, and g is phase angle. ω , B , Φ , and H are single scattering albedo, backscattering function, scattering phase function, and multiple-scattering function, respectively,

and are written as,

$$\omega = \frac{Q_S}{Q_E}, \quad (2)$$

$$B(g) = \exp(-\omega^2/2) \left\{ 1 - \frac{\tan |g|}{2h} [3 - \exp(-h/\tan |g|)] [1 - \exp(-h/\tan |g|)] \right\}, \quad (3)$$

$$\Phi(g) = 1 - 0.4 \cos(g) + 0.25 [1.5 \cos^2(g) - 0.5], \quad (4)$$

$$H(\mu) = \frac{1 + 2\mu}{1 + 2\chi\mu}. \quad (5)$$

Q_S , and Q_E are scattering efficiency and extinction efficiency, respectively, which can be calculated using the Mie theory [14, 17]. Hapke derived simplified analytical solutions, which are functions of internal scattering coefficient s and internal absorption coefficient $\alpha = \frac{4\pi k}{\lambda}$ [10]. The relations are omitted here for brevity. $\chi = (1 - \omega)^{1/2}$, and $h = 0.1$.

The process for determining the optical properties is described as follows. Observing that the derived bi-directional reflectance is a function of the single scattering albedo, thus the single scattering albedo is extracted from the measured bi-directional reflectance. Then, the single scattering albedo relates to the grain size and the optical properties of the material. We assume a representative particle size corresponding to the average of the reported sieve size range for each powder samples: 15 μm for for 0–30 μm separate and 22.5 μm for for 0–45 μm separate. The conversion of the single albedo to the optical constants thus removes the effects of particle size.

3.2. Analysis of radiative transfer in slab media by the two-flux approximation

Consider the problem of light incident onto a pellet medium. Treating the pellet as a one-dimensional plane-parallel layer of an absorbing, refracting, and scattering medium, as shown in Fig. 5, the two-flux approximation method is employed to analyze the radiative transfer in the medium. The method is subject to the following assumptions: (i) the investigated materials are homogeneous and isotropic, (ii) radiation is isotropic scattered, (iii) the surface is isotropic and diffuse, (iv) the sample is optically thick. The directional-hemispherical reflectance is then obtained as [6, 8]:

$$R_{d-h} = R_1 + (1 - R_1) \frac{\gamma}{2n^2} \frac{\omega_s}{1 - \omega_s} \frac{\kappa^2}{(1 + \kappa) \left(\frac{2\kappa}{1 + \eta} + \kappa \right)}, \quad (6)$$

where

$$\kappa^2 = \frac{4}{(1 + \eta)^2} \frac{1 - \omega_s}{1 - \omega_s \eta}, \quad (7)$$

$$\gamma = \frac{1 - R_1}{1 + R_1}, \quad (8)$$

$$\eta = \sqrt{1 - \frac{1}{n^2}}. \quad (9)$$

$\omega_s = \frac{s}{s + \alpha}$ is the scattering albedo of the slab medium. The interface reflectivity R_1 is obtained by averaging the Fresnel reflectivity over the hemisphere,

$$R_1 = \frac{1}{2} + \frac{(3n + 1)(n - 1)}{6(n + 1)^2} + \frac{n^2(n^2 - 1)^2}{(n^2 + 1)^3} \ln \left(\frac{n - 1}{n + 1} \right) - \frac{2n^3(n^2 + 2n - 1)}{(n^2 + 1)(n^4 - 1)} + \frac{8n^4(n^4 + 1)}{(n^2 + 1)(n^4 - 1)^2} \ln n. \quad (10)$$

It is observed that the directional-hemispherical reflectance is a function of the refractive index n . Thus, the refractive index n is identified from fitting with the measured reflectance spectra of the pellet material. The value is then used in the previous inverse process based on the Hapke radiation model for identifying the absorptive index k . The whole process containing these two steps is iterated until changes in n and k are insignificant.

3.3. Analysis of radiative transfer in multi-layer stratified media by the electric field transfer matrix

When discussing reflection from a film layer on top of a distinct substrate, reflection and transmission of electromagnetic radiation from one or more phases in the form of stratified medium of multiple layers are investigated (see Fig. 6). Specifically, the medium system of ilmenite-pigmented film deposited on aluminium substrate in this work is treated as a N -phase ($N = 3$) stratified medium, which consists of air, ilmenite-pigmented low-density polyethylene film, and aluminium substrate. This results in $N - 1$ surfaces of discontinuity at $z = z_k$ ($k = 1, 2, \dots, N - 1$). Each Phase ($z_{k-1} < z < z_k$) is characterised with its individual thickness h_j , dielectric constant ϵ_j , permeability μ_j , conductivity σ_j , complex index of refraction $m_j = n_j + ik_j$, and transfer matrix M_j . The tangential fields at the first boundary, z_1 , are related to those at the final boundary, z_{N-1} , by [9]

$$\begin{bmatrix} U_1 \\ V_1 \end{bmatrix} = M_2 M_3 \cdots M_{N-1} \begin{bmatrix} U_{N-1} \\ V_{N-1} \end{bmatrix} = M \begin{bmatrix} U_{N-1} \\ V_{N-1} \end{bmatrix}, \quad (11)$$

where U_k and V_k are the tangential components of the electric (E) or magnetic (H) field amplitudes at the k -th boundary. Specifically, for parallel (\parallel) polarization, $U_k = H_y^0$, and $V_k = E_x^0$, for perpendicular (\perp) polarization, $U_k = E_y^0$, and $V_k = H_x^0$. M_j is the characteristic matrix for the

j -th layer, it is written as

$$M_j = \begin{bmatrix} \cos \beta_j & \frac{-i}{p_j} \sin \beta_j \\ -ip_j \sin \beta_j & \cos \beta_j \end{bmatrix}, \quad (12)$$

and

$$M_j = \begin{bmatrix} \cos \beta_j & \frac{-i}{q_j} \sin \beta_j \\ -iq_j \sin \beta_j & \cos \beta_j \end{bmatrix}, \quad (13)$$

for TE and TM polarization, respectively, where $\beta_j = \frac{2\pi}{\lambda} m_j \cos \theta_j h_j$, $p_j = (\epsilon_j/\mu_j)^{1/2} \cos \theta_j$, and $q_j = (\mu_j/\epsilon_j)^{1/2} \cos \theta_j$.

The reflectance is thus obtained as

$$R_{\parallel} = \left| \frac{H_{y1}^{0r}}{H_{y1}^{0t}} \right|^2 = \left| \frac{(M_{11} + M_{12}q_N)q_1 - (M_{21} + M_{22}q_N)}{(M_{11} + M_{12}p_N)q_1 + (M_{21} + M_{22}q_N)} \right|^2, \quad (14)$$

$$R_{\perp} = \left| \frac{E_{y1}^{0r}}{E_{y1}^{0t}} \right|^2 = \left| \frac{(M_{11} + M_{12}p_N)p_1 - (M_{21} + M_{22}p_N)}{(M_{11} + M_{12}p_N)p_1 + (M_{21} + M_{22}p_N)} \right|^2, \quad (15)$$

where M_{ij} are the elements of the matrix M in Eq. (11), superscripts r and t represent reflected and transverse components. Employing the optical properties of ilmenite determined from the previous subsections using the Hapke and two-flux approximation models, the reflectance and thus emissivity/absorptivity of the fabricated ilmenite-pigmented low-density polyethylene film on aluminium is obtained.

4. Results and discussions

The bi-directional reflectance for the particulate media of the $<30 \mu\text{m}$ and $<45 \mu\text{m}$ grain size fractions of ilmenite are used in the Hapke radiative transfer model to determine the absorptive index k . The refractive index n is extracted from the directional-hemispherical reflectance for the pellet medium of ilmenite by an inverse process based on the two-flux approximation radiative transfer model. It is found that the internal scattering coefficient, s , in the Hapke model plays an important role in the optical property identification. In the absence of a prior understanding of the material, the parameter is set to a small or even zero constant value across the entire spectral range in the standard approach [15, 21]. Accurate determination of the optical constants has been provided for materials showing weak absorption characteristics. However, inaccuracies in estimates of the absorptive index are observed to be introduced in regions of strong absorption. Thus, the determination of the appropriate value of the internal scattering coefficient is required to accurately obtain the optical properties of absorbing materials.

4.1. Constant internal scattering coefficient

First, assuming that the internal scattering coefficient s is independent of the wavelength, the calculation procedure of determining the optical constants is performed for employing the values of $s = 10^{-14}, 10^{-7}, 10^{-3}, 10^{-2}, 10^{-1}, 10$ (units of μm^{-1}). The refractive index is then determined and plotted in Fig. 7. It is seen that values of the refractive index n obtained show negligible difference for $s < 10^{-2} \mu\text{m}^{-1}$. The determined absorptive index is also plotted in Fig. 8. The values of the absorptive index k align very well when employing small values of $s < 10^{-1} \mu\text{m}^{-1}$. In addition, reflectance spectra are reconstructed using optical properties determined to examine the fitting performance. Good agreement is achieved when employing these small internal scattering coefficient values. Then, further scrutiny is engaged by increasing the values of the internal scattering coefficient. Specifically, with the internal scattering coefficient increasing to $s = 10^{-1} \mu\text{m}^{-1}$, the values of n deviate from those of employing smaller s . When observing the corresponding phenomenon in the absorptive index, it is found that considerably higher values are retrieved when s is increased to $10 \mu\text{m}^{-1}$. The calculated reflectance spectra also correspondingly start to show poor agreement with the measurement reflectance data. Combing both of the analyses for n and k , it is concluded that the internal scattering coefficient for ilmenite material is small enough in the range of $s < 10^{-2} \mu\text{m}^{-1}$, and become large in the range of $s > 10^{-1} \mu\text{m}^{-1}$. The accurate fitting of calculation with measurement reflectance data across the entire spectral range requires a small enough value of the internal scattering coefficient, which is corroborated in relevant studies [20, 21].

Employing the determined optical constants using small internal scattering coefficient of $s = 10^{-7} \mu\text{m}^{-1}$, the emissivity/absorptivity of the $50 \mu\text{m}$ -thick ilmenite-pigmented film on aluminium is calculated and shown in Fig. 9. Comparing with the measurement data, it is observed that a good agreement in the spectral range of $\lambda < 13 \mu\text{m}$ is achieved, although acceptable discrepancy exists. However, an overwhelmingly underestimation in emissivity and absorptivity is found in the spectral range of $> 13 \mu\text{m}$. This phenomenon agrees with the characteristics of the standard Hapke radiation model, which is known to be incapable of addressing the strong absorption features of absorbing materials.

4.2. Wavelength-dependent internal scattering coefficient

To resolve the issue of underestimation in the infrared absorption recognized above, assumption of constant value of the internal scattering coefficient across the entire spectral range, which is usually employed for unknown materials in the standard approach, is required to be released. Fortunately, more supporting information on absorption features of ilmenite material is available in a relevant study[13]. Ilmenite powder having an average particle diameter smaller than $5 \mu\text{m}$ was deposited as a film on a conventional rock salt window for infrared absorption investigation

and the transmission spectra are shown in Fig.10. The curves have shown high transmission in the spectral range of 7–13 μm , and are observed to absorb strongly over spectral range starting at 13 μm . Thus, in the current study, only wide band specifications ($\lambda < 7 \mu\text{m}$, $7 \mu\text{m} < \lambda < 13 \mu\text{m}$, $\lambda > 13 \mu\text{m}$) are taken into account for revealing distinct, wavelength-dependent absorbing features considering that much better resolution spectral data are not available. The internal scattering coefficient in regions of weak absorption require a low value to generate the phenomenon associated with the measured reflectance data. In the regions of stronger absorption, the trend associated with the reflectance spectra require larger values of the internal scattering coefficient. Thus, modification of constant values of s is made by specifying large values on the internal scattering coefficient in the spectral range of strong absorption when the wavelength is smaller than 7 μm and larger than 13 μm . As discussed and concluded in the previous subsection, $s > 10^{-1} \mu\text{m}^{-1}$ is found to be the delineation between small and large values of s . Thus, in the spectral range of strong absorption ($\lambda < 7 \mu\text{m}$ and $\lambda > 13 \mu\text{m}$), values of $s = 10, 50, 100, 1000 \mu\text{m}^{-1}$ are employed in the calculation for determining the optical properties. The wavelength-dependent internal scattering coefficient is then plotted in Fig. 11. The individual optical determination by employing the varied internal scattering coefficient is subsequently conducted. Then, the emissivity/absorptivity of the film system using the determined optical properties is calculated. The curve shown in Fig. 12 is obtained by employing $s_1 = 10 \mu\text{m}^{-1}$ in regions of strong absorption. It is clear that the underestimation of absorption in the infrared region remains. Increasing the value to $s_2 = 50 \mu\text{m}^{-1}$, this issue is resolved and accurate prediction of emissivity/absorptivity in the region is achieved (see Fig. 13). Additionally, it is found that reconstructed reflectance spectra agree well with those of measurements. A continuing increase in the internal scattering coefficient (s_3, s_4) in regions of strong absorption gradually fails both the absorption modification in the infrared regions and the fitting agreement in reflectance spectra. This thus shows accuracy and validity for determination of the internal scattering coefficient and optical properties.

4.3. Optical properties

Employing the wavelength-dependent internal scattering coefficient of $s_2 = 50$ and $10^{-7} \mu\text{m}^{-1}$ in regions of strong absorption and high transmission, respectively, the optical properties of ilmenite material are thus obtained and shown in Fig. 14. The value of the refractive index n varies weakly on the wavelength. In contrast, a more pronounced change in the absorptive index k with the wavelength is observed. Specifically, low values of the absorptive index k on the magnitude of 10^{-2} in the atmospheric window spectral range are observed, which results in high transmission of ilmenite in the spectral range. Furthermore, in the strong absorption infrared spectral range starting from 13 μm , values of the absorptive index k are higher than 0.1, which is also in agreement with the statement of $k > 0.1$ for absorbing ilmenite demonstrated in the study [10].

5. Conclusions

We recognize the necessity of determination for optical properties of absorbing ilmenite and issues associated with bi-directional reflectance spectroscopy identification method used in this work. The spectroscopy consists of measurements on reflectance and analysis of radiative transfer in particulate media by multiple scattering theory (Hapke radiative transfer model). One issue encountered in this standard approach is the handling of the refractive index n , which is assuming a constant value subject to a prior understanding of the materials, and subsequently employing a subtractive Kramers–Kronig analysis to allow for wavelength-dependent values. However, this results in fundamental insensitivity to spectral features and changes in the absorptive index k across the entire spectral range. Another issue is that the standard approach provides a poor determination of the optical properties in the infrared regions where absorbing materials exhibit strong absorption specifications.

In this work, we resolve these issues by complementing distinct radiative transfer analysis and then identify the optical properties of ilmenite material. We supplement the Hapke model with an additional analysis for the problem of radiative transfer in a slab medium of the material to solve the issue of two unknowns n and k and fundamental insensitivities associated with the subtractive Kramers–Kronig analysis. The two-flux approximation is used in solving and analyzing the radiative transfer within the slab medium. Aiding with the transmission spectra of the particulate thin film, the internal scattering coefficient parameter of grains which is neglected in the standard approach is found to be the key in identifying the absorption features of materials. The validation of the combined spectroscopy proposed in this work and the determination of the internal scattering coefficient are achieved by scrutinizing the absorptivity/emissivity of the multi-layer medium of the material, which is modelled as a N -phase stratified medium and analyzed by investigating the propagation of electromagnetic radiation within.

The results show that a constant internal scattering coefficient, which is employed in the standard bi-directional reflectance spectroscopy, results in a poor determination of the optical properties in infrared regions where absorbing materials exhibit strong absorption specifications. Observing the absorption and transmittance features from the transmission spectrum of the ilmenite power film, a wavelength-dependent internal scattering coefficient of $s = 50$ and $10^{-7} \mu\text{m}^{-1}$ in regions of strong absorption and high transmission, respectively, is obtained. The value of the refractive index n varies weakly on the wavelength. While, a more pronounced change in the absorptive index k with the wavelength is observed. Specifically, the low values of the absorptive index k on the magnitude of 10^{-2} in the atmospheric window spectral range corroborate the phenomenon of high transmission of ilmenite in this spectral range. In the strong absorption infrared spectral range starting from $13 \mu\text{m}$, the values of the absorptive index k are higher than 0.1, which corroborate strong absorption of the material.

References

- [1] H. Aasen, E. Honkavaara, A. Lucieer, and P. J. Zarco-Tejada. Quantitative remote sensing at ultra-high resolution with UAV spectroscopy: a review of sensor technology, measurement procedures, and data correction workflows. *Remote Sensing*, 10(7):1091, 2020.
- [2] K. Bell and P. Reza. Non-contact reflection-mode optical absorption spectroscopy using photoacoustic remote sensing. *Optics Letters*, 45(13):3427–3430, 2020.
- [3] M. A. Butt, S. N. Khonina, and N. L. Kazanskiy. Recent advances in photonic crystal optical devices: A review. *Optics & Laser Technology*, 142:107265, 2021.
- [4] W. Calvin. Additions and corrections to the absorption coefficients of CO₂ ice: Applications to the Martian south polar cap. *Journal of Geophysical Research: Solid Earth*, 95(B9):14743–14750, 1990.
- [5] I. Carusotto, A. A. Houck, A. J. Kollár, P. Roushan, D. I. Schuster, and J. Simon. Photonic materials in circuit quantum electrodynamics. *Nature Physics*, 16:268–279, 2020.
- [6] J. Chen, A. Riaz, M. Taheri, A. Kumar, J. Coventry, and W. Lipiński. Optical and radiative characterisation of alumina–silica based ceramic materials for high-temperature solar thermal applications. *Journal of Quantitative Spectroscopy & Radiative Transfer*, 272:107754, May 2021.
- [7] R. N. Clark and T. L. Roush. Reflectance spectroscopy: quantitative analysis techniques for remote sensing applications. *Journal of Geophysical Research: Solid Earth*, 89(B7):6329–6340, 1984.
- [8] L.A. Dombrovsky, J.H. Randrianalisoa, and D. Baillis. Modified two-flux approximation for identification of radiative properties of absorbing and scattering media from directional-hemispherical measurements. *Journal of the Optical Society of America A*, 23(1):91–98, January 2006.
- [9] W.N. Hansen. Electric fields produced by the propagation of plane coherent electromagnetic radiation in a stratified medium. *Journal of the Optical Society of America*, 58(3):380–390, 1968.
- [10] B. Hapke. Bidirectional reflectance spectroscopy: 1. Theory. *Journal of Geophysical Research*, 86(B4):3039–3054, 1981.
- [11] H.G. Tompkins. *A User’s Guide to Ellipsometry*. Academic Press, San Diego, 1993.
- [12] T. Hiroi and C. Pieters. Estimation of grain sizes and mixing ratios of fine powder mixtures of common geologic minerals. *Journal of Geophysical Research*, 99(E5):10867–10879, 1994.
- [13] J.M. Hunt, M.P. Wisherd, and L.C. Bonham. Infrared absorption spectra of minerals and other inorganic compounds. *Analytical Chemistry*, 22(12):1478–1497, 1950.
- [14] J.R. Howell, M.P. Mengüç, K. Daun, and R. Siegel. *Thermal Radiation Heat Transfer*. CRC Press, Boca Raton, 7th edition, 2020.
- [15] P. Lucey. Model near-infrared optical constants of olivine and pyroxene as a function of iron content. *Journal of Geophysical Research*, 103(103):1703–1713, 1998.
- [16] E. J. Milton. Review article principles of field spectroscopy. *Remote Sensing*, 8(12):1807–1827, 1987.
- [17] M.F. Modest and S. Mazumder. *Radiative Heat Transfer*. Academic Press, New York, 4th edition, 2021.
- [18] A.P. Raman, M.A. Anoma, L. Zhu, E. Rephaeli, and S. Fan. Passive radiative cooling below ambient air temperature under direct sunlight. *Nature*, 515:540–544, 2014.
- [19] T. Roush, J. Pollack, F. Witteborn, J. Bregman, and J. Simpson. Ice and minerals on Callisto: A reassessment of the reflectance spectra. *Icarus*, 86(2):355–382, 1990.

- [20] T. Roush, L. Teodoro, D. Blewett, and J. Cahill. Optical constants and diffuse reflectance of opaque minerals: A modelin study using magnetite. *Icarus*, 361:114331, 2021.
- [21] T.L. Roush, F. Esposito, G. Rossman, and L. Colangeli. Estimated optical constants of gypsum in the regions of weak absorptions: Application of scattering theories and comparisons to independent measurements. *Journal of Geophysical Research*, 112(B4):E10003, 2007.
- [22] Y. Shkuratov and Y. Grynko. Light scattering by media composed of semitransparent particles of different shapes in ray optics approximation: consequences for spectroscopy, photometry, and polarimetry of planetary regoliths. *Icarus*, 173:16–28, 2005.
- [23] D. Sun, Y. Zhang, D. Wang, W. Song, X. Liu, J. Pang, D. Geng, Y. Sang, and H. Liu. Microstructure and domain engineering of lithium niobate crystal films for integrated photonic applications. *Light: Science & Applications*, 9(1):197, 2020.
- [24] Y. Zhai, Y. Ma, S. David, D. Zhao, R. Lou, G. Tan, R. Yang, and X. Yin. Scalable-manufactured randomized glass-polymer hybrid metamaterial for daytime radiative cooling. *Science*, 350:1062–1066, 2017.

Figures

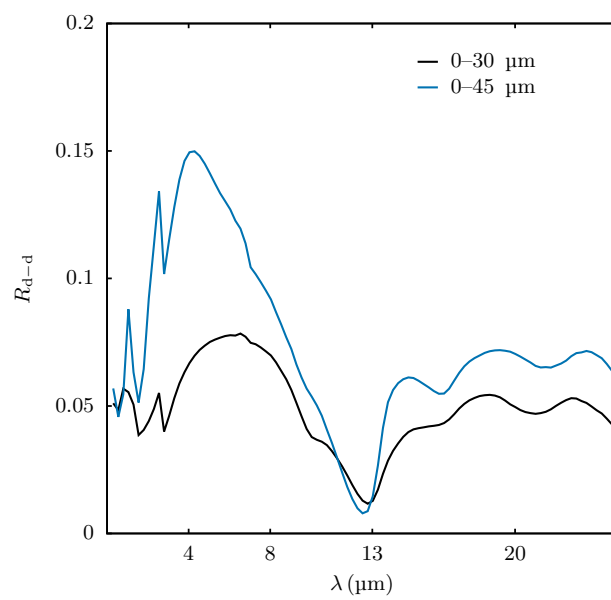


Figure 1: Bi-directional reflectance spectra of particulate ilmenite from RELAB spectral library.

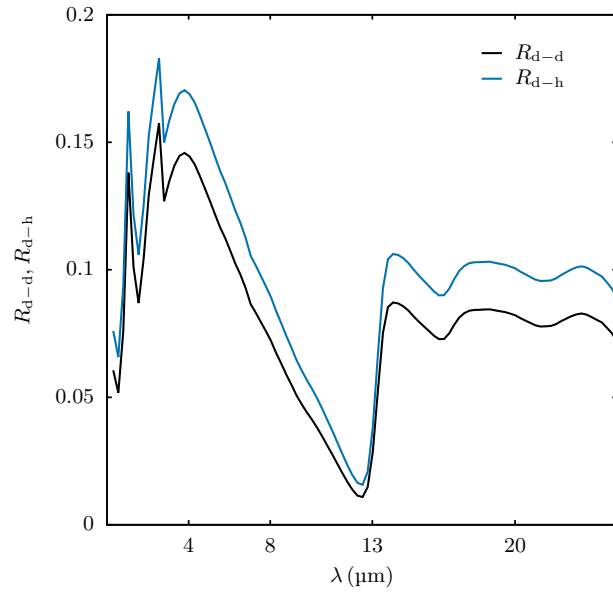


Figure 2: Bi-directional reflectance of pellet ilmenite from RELAB spectral library and calculated directional-hemispherical reflectance employing the Shkuratov and Grynko model [22].

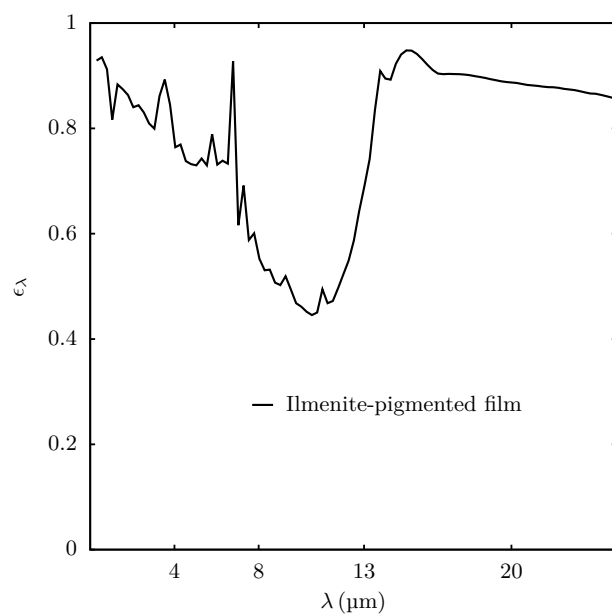


Figure 3: Emissivity/absorptivity of ilmenite-pigmented low-density polyethylene film backed with aluminium substrate.

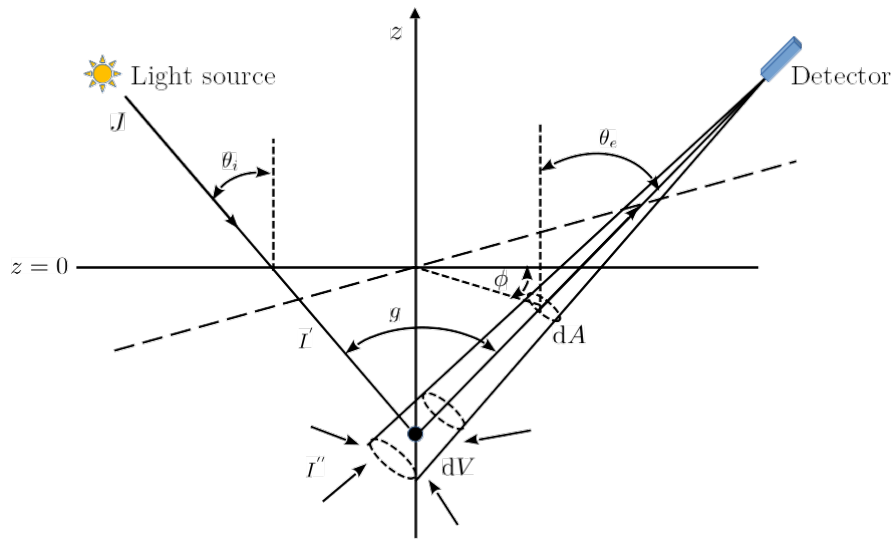


Figure 4: Schematic of the scattering of light from particulate surfaces.

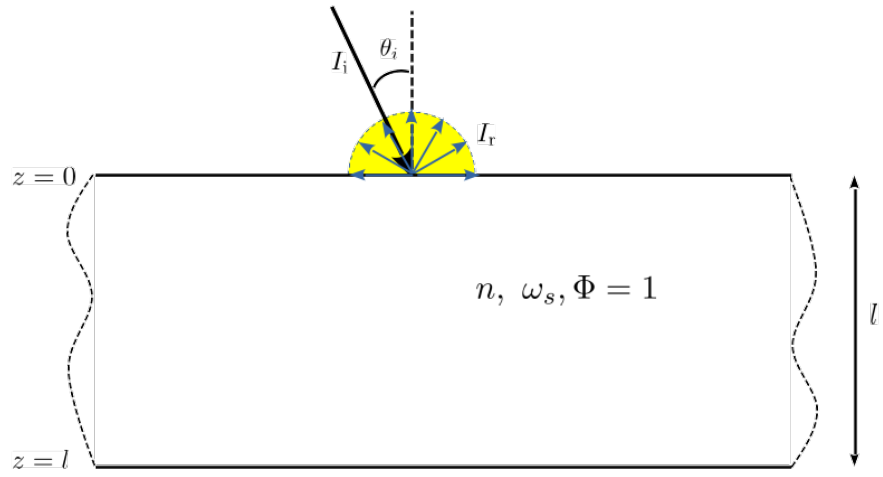


Figure 5: Schematic of a plane-parallel layer of an absorbing, scattering and refracting medium.

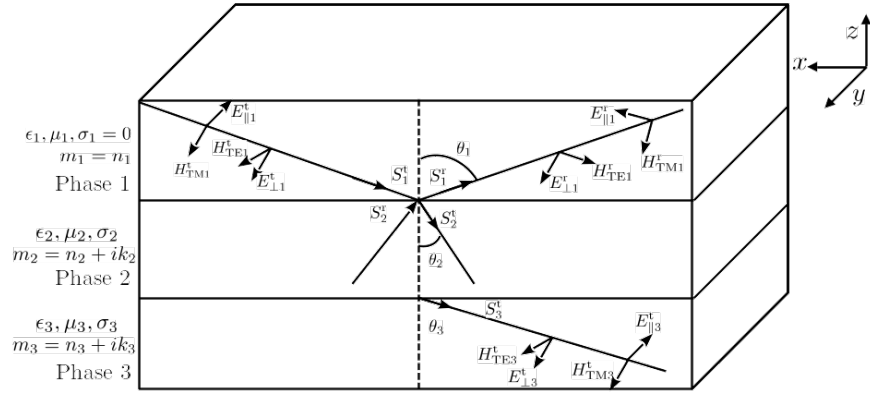


Figure 6: Plane coherent electromagnetic radiation interaction in a three-phase medium.

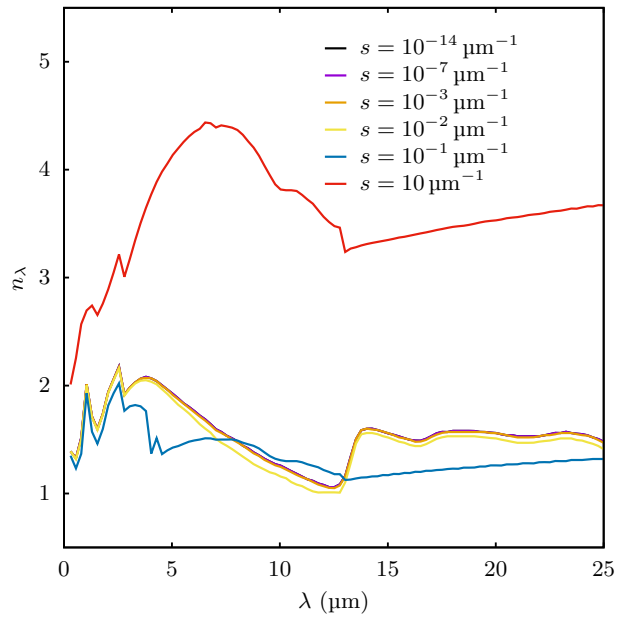


Figure 7: Comparison of the refractive index derived for varying constant internal scattering coefficient.

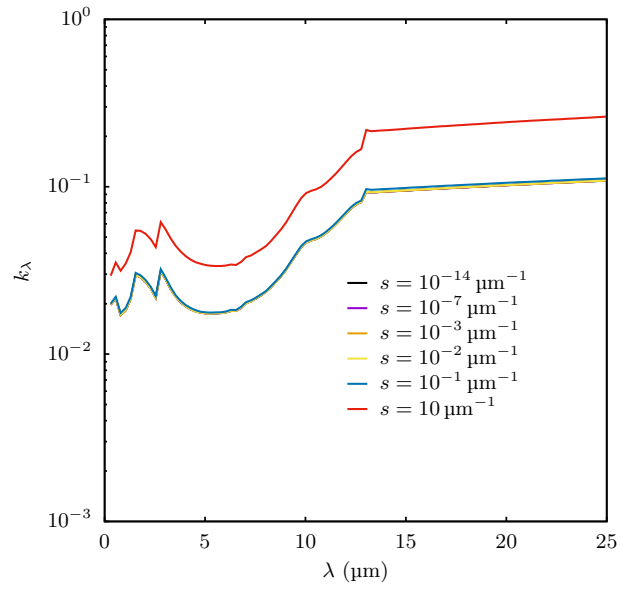


Figure 8: Comparison of the absorptive index derived for varying constant internal scattering coefficient.

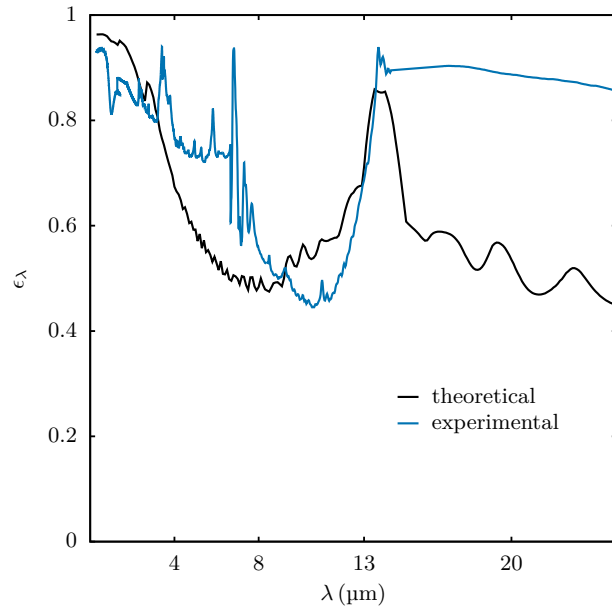


Figure 9: Measured and calculated emissivity/absorptivity of 50 μm -thick ilmenite-pigmented polyethylene film on aluminium substrate by employing the optical constants determined using $s = 10^{-7} \mu\text{m}^{-1}$ in the Hapke model.

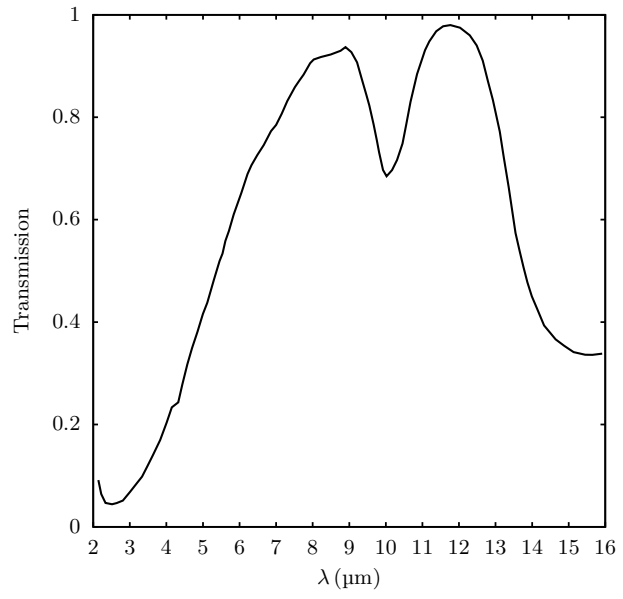


Figure 10: Transmission spectra of ilmenite powder deposited on a conventional rock salt window.

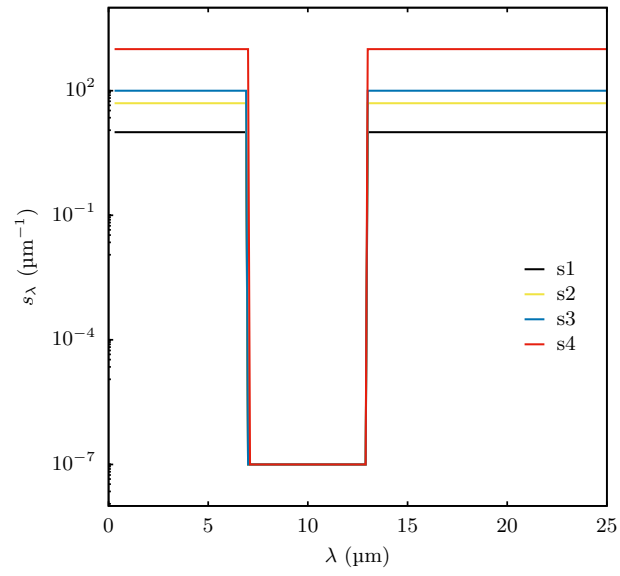


Figure 11: Wide band internal scattering coefficient.

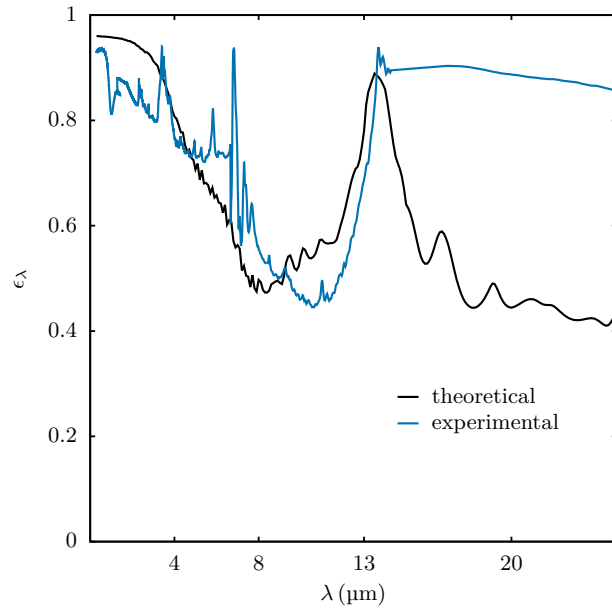


Figure 12: Measured and calculated emissivity/absorptivity of 50 μm ilmenite-pigmented film on aluminium substrate by employing the optical constants determined using wide band internal scattering coefficient of $s_1 = 10 \mu\text{m}^{-1}$ in regions of strong absorption.

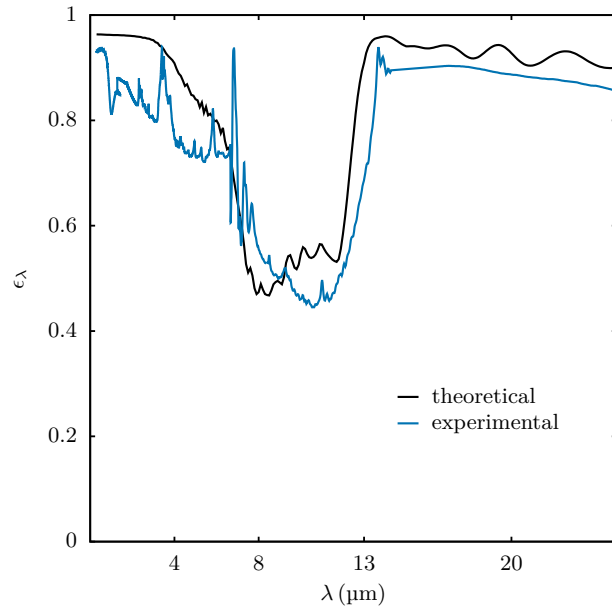


Figure 13: Measured and calculated emissivity/absorptivity of 50 μm ilmenite-pigmented film on aluminium substrate by employing the optical constants determined using wide band internal scattering coefficient of $s_2 = 50 \mu\text{m}^{-1}$ in regions of strong absorption.

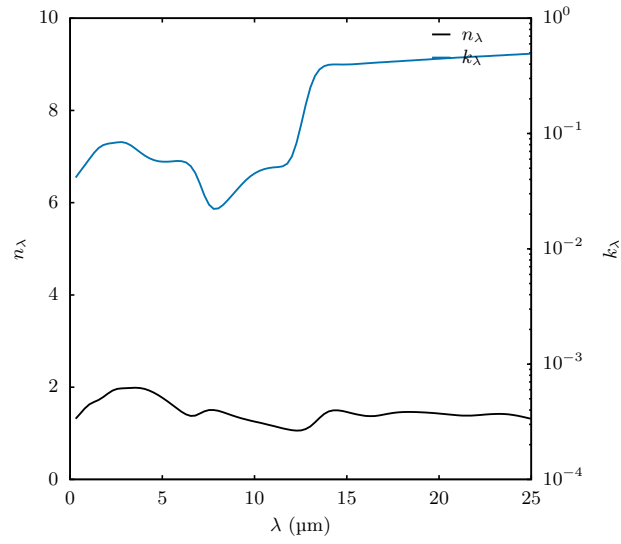


Figure 14: Optical constants of ilmenite material.